Water Vapor Radiometer–Global Positioning System Comparison Measurements and Calibration of the 20 to 32 Gigahertz Tropospheric Water Vapor Absorption Model

S. J. Keihm,[1] Y. Bar-Sever,[2] and J. Liljegren[3]

Collocated measurements of opacity (from water vapor radiometer (WVR) brightness temperatures) and wet path delay (from ground-based tracking of Global Positions System (GPS) satellites) are used to constrain the model of atmospheric water vapor absorption in the 20 to 32 GHz band. A differential approach is presented in which the slope of opacity-versus-wet delay data is used as the absorption model constraint. This technique minimizes the effects of radiometric calibration errors and oxygen model uncertainties in the derivation of a best-fit vapor absorption model. A total of approximately 5 months of data were obtained from two experiment sites. At the Cloud and Radiation Testbed (CART) site near Lamont, Oklahoma, three independent WVRs provided near-continuous opacity measurements over the interval from July through September 1998. At NASA's Goldstone tracking station in the California desert, two WVRs obtained opacity data over the September through October 1997 interval. At both sites, a GPS receiver and surface barometer obtained the data required for deriving the zenith wet delays over the same time frames.

Measured values of the opacity-versus-wet delay slope parameter were obtained at four WVR frequencies (20.7, 22.2, 23.8, and 31.4 GHz) and compared with predictions of three candidate absorption models referenced in the recent literature. With one exception, all three models provide agreement within approximately 5 percent of the opacity-versus-wet delay slope measurements at all WVR frequencies at both sites. One model provides agreement for all channels at both sites to the 2 to 3 percent level. This accuracy is sufficient to meet the requirements of the tropospheric calibration system now being deployed at Goldstone to support the Cassini Gravitational Wave Experiment.

---

[1] Microwave and Lidar Technology Section.

[2] Tracking Systems and Applications Section.

[3] Environmental Research Division, Argonne National Laboratory, Argonne, Illinois.

The research described in this publication was carried out by the Jet Propulsion Laboratory, California Institute of Technology, under a contract with the National Aeronautics and Space Administration.

I. Introduction

Ground-based and satellite microwave radiometer measurements of atmospheric vapor burden and vapor-related quantities such as the wet path delay are subject to three distinct types of error sources: instrument calibration, modeling, and retrieval algorithm. Instrument calibration uncertainties include both offset and gain errors as well as unmonitored drifts in these parameters. Modeling errors reflect the uncertainty in the computation of theoretical microwave brightness temperatures and opacities (observables) given a complete atmospheric profile of temperature, pressure, and emitter (oxygen, water vapor, cloud liquid) densities. This forward model error is due mainly to uncertainties in the absorption models for atmospheric oxygen and water vapor in the 20 to 32 GHz spectral band most often utilized by tropospheric-sensing water vapor radiometers (WVRs). Comparisons of vapor absorption models commonly cited in the literature suggest that the uncertainty is in the 5 to 10 percent range [1].[4] Retrieval algorithm errors are due to the non-unique mapping of WVR observables to the desired retrievables (e.g., vapor burden or wet path delay); i.e., an infinite number of atmospheric states (profiles of temperature, pressure, vapor, and liquid density) can produce a given set of WVR brightness temperatures. The most probable atmospheric state, derived from a priori statistics as well as the observables, will contain errors in the retrieved vapor abundance even for zero error observables and a perfect forward model.

In terms of absolute accuracy, vapor absorption model uncertainties of ± 5 percent can dominate the WVR vapor measurement error budget, especially for high humidity conditions. For global-average humidity conditions over the oceans, this is the case for satellite microwave measurements of the wet path delay, such as performed by the TOPEX/Poseidon microwave radiometer [2]. For most ground-based weather-monitoring operations, 5 percent accuracy in retrieved water vapor products is sufficient. However, for applications requiring higher precision, a 5 percent absorption model uncertainty can represent a significant component in the vapor measurement error budget. Such is the case for the tropospheric calibration system [3] designed to support the Cassini radio science Gravitational Wave Experiment (GWE) [4]. This calibration system consists primarily of a highly stable advanced water vapor radiometer (AWVR) [5] and is intended to provide a precise measure of the line-of-sight, water-vapor-induced signal delay in the Doppler tracking of the Cassini spacecraft at the NASA Goldstone station. High precision is required to remove the effects of the rapidly fluctuating vapor-induced delay in order to isolate the Doppler signal variations expected to be characteristic of gravitational waves. Analysis of the complete error budget for the tropospheric calibration system reveals that 2 to 3 percent accuracy in the water-vapor absorption model is required to meet Cassini GWE requirements.[5]

To address the absorption model issue, we have conducted a campaign of comparison studies between WVR-derived zenith opacities and collocated measurements of the zenith wet path delay provided by a Global Positioning Satellite (GPS) receiver. The wet path delay is highly correlated with vapor abundance so that comparisons of WVR-derived opacities with GPS-derived wet delays can be used to constrain the water vapor absorption model. The experimental data were obtained at two sites: NASA's Goldstone tracking station (GTS) in the Mojave Desert, over a 2 month interval in 1997, and the Cloud and Radiation Testbed (CART) site, operated by the Department of Energy at Lamont, Oklahoma, over a 3 month interval in 1998.

In Section II, we provide background on current versions of the atmospheric vapor absorption model, their uncertainties, and standard methods used in the past to improve model accuracy. In Section III, we describe a new approach for constraining the vapor absorption model using WVR and GPS measurements. This method minimizes the effects of WVR calibration and oxygen model uncertainties on the derived absorption model. In Section IV, the GPS and WVR instrumentation and data processing are described, including scatter plots of the WVR-derived opacities versus GPS-derived wet delays at both experiment

[4] S. J. Keihm, *Water Vapor Radiometer Intercomparison Experiment. Platteville, Colorado 1991*, JPL D-8898 (internal document), Jet Propulsion Laboratory, Pasadena, California, 1991.

[5] R. Linfield, "Error Budget for JPL's WVR-Based Troposphere Calibration System," JPL Interoffice Memorandum 335.1-98-014 (internal document), Jet Propulsion Laboratory, Pasadena, California, November 3, 1998.

sites. Section V describes the regression analysis performed on the opacity-versus-wet delay data sets and evaluates the slope results in terms of vapor absorption model constraints. In Section VI, we summarize our results, assess the accuracy of the derived "best" model, and recommend future work for improvement of the tropospheric calibration system at Goldstone.

II. Background

Over the past 25 years of rapidly evolving microwave remote sensing instrumentation, numerous models of the 20 to 32 GHz water vapor absorption have been proposed and utilized in vapor-related retrieval algorithms. In the 1978 to 1995 interval, many investigators adopted models proposed by Waters [6] and Liebe [7–9] based primarily on laboratory measurements. These models differed by as much as 10 percent in the 20 to 32 GHz band, due primarily to differences in the assumed line shape models. Models were frequently tested by comparing radiosonde-based calculations of 20 to 32 GHz brightness temperatures with collocated radiometric measurements [10–14]. These comparisons were primarily limited by 5 to 10 percent uncertainties in the calibration accuracy of the radiosonde vapor density determinations, both random variations between individual radiosondes [15–17], and especially systematic biases that depended on radiosonde manufacturer and lot number [18].

Over the past 10 years, variations of the Liebe models have been favored, based primarily on validations of the Van Vleck–Weiskopf line shape for the 22 GHz absorption feature [12,19]. Although later versions of the Liebe model contain slight modifications to the 22 GHz vapor absorption feature, a number of investigators still favor the 1987 version. For the present work, we examine three candidate models for the 20 to 32 GHz vapor absorption spectrum. One is the equivalent of the Liebe 1987 model, referred to as Liebe87. The other two are based on a parameterization of the Liebe model and are intended to apply only to the 20 to 32 GHz spectral range utilized by most current water vapor radiometers. The parameterization used for all three models is presented in the Appendix and contains three variable coefficients (C_L, C_W, and C_C) that allow scaling of the line strength, line width, and continuum terms. Selection of $CL = C_W = 1.00$ and $C_C = 1.20$ produces an absorption spectrum [Fig. 1(a)] within 0.5 percent of the original Liebe87 model. Note in Fig. 1(a) the pressure broadening effect, producing higher absorption for lower pressures at the 22.2 GHz line center, and the opposite effect in the wing region near 31 GHz. As shown in Section V, this effect has significant impact on site/seasonal differences and year-to-year variability at the 22.2 and 31.4 GHz WVR frequencies.

Selection of $C_L = 1.05$, $C_W = 1.00$, and $C_C = 1.30$ produces our second candidate model, which we refer to as the JPL model since it is largely based on Platteville, Colorado, radiosonde comparisons with JPL WVRs[6] and was utilized in the JPL development of the TOPEX microwave radiometer path delay retrieval algorithm [2]. Our third candidate absorption model, produced by the selection of $C_L = 1.064$, $C_W = 1.066$, and $C_C = 1.237$, was derived from WVR–radiosonde comparisons from the sea-level sites of San Diego, California, and West Palm Beach, Florida, [20] and is referred to as the Cruz model. Differences relative to the Liebe87 model are shown in Fig. 1(b) for sea-level conditions. Note that the JPL model shows a nearly flat spectrum relative to Liebe87, having been produced by a 5 percent increase in line strength and an 8.3 percent increase in the continuum component. The Cruz model, with a 6.5 percent increase in both line strength and line width, shows a large 18 to 32 GHz spectral signature relative to the Liebe87 and JPL models. Note that all three candidate models contain the same exponential coefficients for temperature dependencies as the original Liebe87 model. Thus, we are testing models that differ only in the magnitudes of the line strength, line width, and continuum terms. Efforts to refine other model coefficients related to temperature and pressure dependencies are probably not warranted by the current set of WVR–GPS comparison measurements.

[6] S. J. Keihm, op cit.

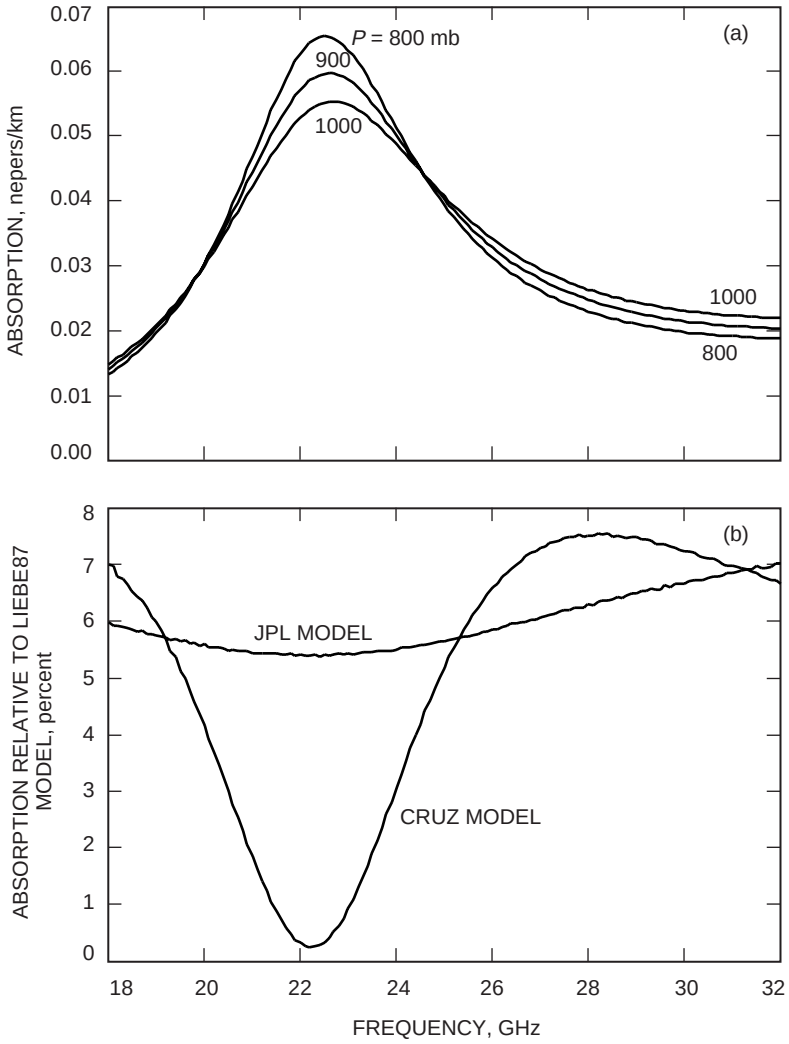

Fig. 1. 18 to 32 GHz vapor absorption for temperature = 290 K and vapor density = 10 g/m^3: (a) a sample of the water vapor absorption coefficient spectrum near the 22 GHz line based on the 1987 model of Liebe, illustrating the pressure-broadening effect and (b) the difference spectra of the JPL and Cruz vapor absorption models relative to Liebe87 for pressure = 1000 mb.

III. Theoretical Approach

For the purposes of absorption model calibration, radiosondes have the advantage of providing a detailed atmospheric profile of temperature and vapor density, from which model-dependent brightness temperatures can be computed and compared directly with coincident WVR measurements. The main limitations of radiosonde comparisons are low data rate (typically two per day for radiosonde launches), poor precision of the radiosonde vapor density measurements, and systematic biases between the calibration of different humidity sensor types [14] and sensors from different manufactured lots and ages [18]. Offset uncertainties of 5 percent in measured vapor burden cannot be ruled out for any specific archive of radiosonde measurements. Thus, even for perfectly calibrated WVR measurements under clear conditions, comparisons with radiosondes cannot provide vapor absorption model calibration to better than the 5 percent confidence level. WVR offset and gain errors further increase this uncertainty by amounts that depend on the vapor burden.

An alternative to radiosondes for an independent measurement of integrated vapor and the related wet delay is GPS. Radio transmissions from GPS satellites are delayed by the neutral atmosphere prior to reception on the ground. Several GPS satellites at various elevations and azimuths are simultaneously visible from a given ground station at all times. The tracking information afforded by this rich spacecraft geometry can be exploited to solve for key attributes of the tropospheric delay, in particular the total zenith delay. Conventionally, the line-of-sight tropospheric delays to each GPS satellite are mapped to zenith, and a single zenith delay parameter is estimated at each epoch. Bar-Sever et al. [21] demonstrated the benefits from adding the estimation of horizontal gradients of tropospheric path delay. The total tropospheric delay that directly is estimated from the GPS data can be separated into two components: a delay due to the dry gases in the troposphere and the non-dipole moment of water vapor refractivity, denoted as zenith hydrostatic delay, and a delay due to the dipole component of water vapor refractivity, denoted as zenith wet delay. The zenith hydrostatic delay can be accurately inferred from precise measurements of surface pressure [22] and removed from the total delay estimates. The resulting wet zenith delay estimates, conventionally given in terms of the equivalent path length, have been the subject of intense validation campaigns during the past 5 to 10 years and have been demonstrated to be 3 to 7 mm accurate [21,23–25]. Most importantly, the accuracy of the GPS estimates of wet delay is highly insensitive to the size of the measured delay, as the only mechanism capable of introducing a scale error, namely the tropospheric mapping function, is much less than 1 percent in error at elevation angles of 7 deg and above [26]. This is an extremely important point in support of the approach presented below to more accurately constrain the atmospheric vapor absorption model using WVR–GPS comparisons.

The link between wet path delay, vapor burden, and WVR-measured brightness temperatures and opacities is revealed in the following equations. The defining equation for the wet delay, PD, utilizes the laboratory measurements of Boudouris [27] to relate the vapor-induced component of refractivity to vapor density, ρ_v, and Kelvin temperature, T:

$$PD = 1.763 \times 10^{-3} \int_0^H \frac{\rho_v}{T} dz \tag{1}$$

where ρ_v is in g/m^3; PD has the units of the incremental vertical path, dz; and the integral extends from the surface to the effective top of the emitting atmosphere, H. Extensive evaluation of the numerous experimental and theoretical determinations of the vapor-induced refractivity component indicates that the relationship expressed in Eq. (1) is accurate to the 0.5 percent level [28].

The ground-based WVR zenith brightness temperature measurements depend on all significant atmospheric emitters and the temperature profile as expressed in the equation for non-scattering radiative transfer through the atmosphere:

$$TB(\nu) = \int_0^H \alpha_\nu \times T(z) \times \exp\left(-\int_0^z \alpha_\nu(z')\, dz'\right) dz + T_{\cos} \times \exp(-\tau_\nu) \tag{2}$$

where $\alpha_\nu(z)$ is the frequency-dependent atmospheric absorption at frequency ν in nepers/km; $T_{\cos}$ is the cosmic background temperature; and $\tau_\nu = \int_0^H \alpha_\nu(z) dz$ is the total atmospheric opacity. As the opacity approaches unity for high humidity conditions, saturation effects lead to non-linear variations of TB with vapor abundance. To mitigate this effect, measured brightness temperatures are converted to opacities using a simplified form of Eq. (2). The atmospheric emission integral in Eq. (2) can be removed by defining a mean radiating temperature,

$$T_{MRT}(\nu) = \frac{\int_0^H \alpha_\nu \times T(z) \times \exp\left(-\int_0^z \alpha_\nu(z')\, dz'\right) dz}{\int_0^H \alpha_\nu \times \exp\left(-\int_0^z \alpha_\nu(z')\, dz'\right) dz} \tag{3}$$

yielding

$$TB(\nu) = T_{MRT} \times \left(1 - \exp(-\tau_\nu)\right) + T_{\cos} \times \exp(-\tau_\nu) \tag{4}$$

T_{MRT} typically varies over the range from 260 to 290 K, dependent primarily on lower troposphere temperatures. Correlations with surface temperature allow estimates of T_{MRT} to be made that reduce the rms uncertainty in T_{MRT} to approximately 1 percent (3 K) for a specific site. With the T_{MRT} estimate from surface temperature, the radiometric brightness temperature measurements can be readily converted to opacity from Eq. (4):

$$\tau_\nu = ln\left(\frac{T_{MRT} - T_{\cos}}{T_{MRT} - TB(\nu)}\right) \tag{5}$$

For clear conditions, the relevant atmospheric emitters are oxygen and water vapor, and the total absorption can be expressed as

$$\alpha_\nu(z) = \alpha_{ox}(z) + \alpha_{vap}(z) = \rho_{ox}(z) \times \kappa_{ox}(z) + \rho_{vap}(z) \times \kappa_{vap}(z) \tag{6}$$

where κ_{ox} and κ_{vap} are the mass absorption coefficients for oxygen and water vapor, dependent on height through temperature and pressure variations, and ρ_{ox} and ρ_{vap} are the oxygen and water vapor densities. Oxygen is well mixed in the troposphere, with absorption properties completely determined by the pressure and temperature profiles. For frequencies near the 22.2 GHz water vapor line, the oxygen contribution in Eq. (2) is small (relative to the vapor component) and nearly constant for a specific site. Thus, WVR-derived opacities will vary linearly with water vapor burden, as will the wet delay.

The correlation between opacity and the wet delay is demonstrated in Fig. 2, derived from application of Eqs. (1) through (6) to 1995 through 1999 cloud-free radiosonde profiles from the Lamont, Oklahoma,

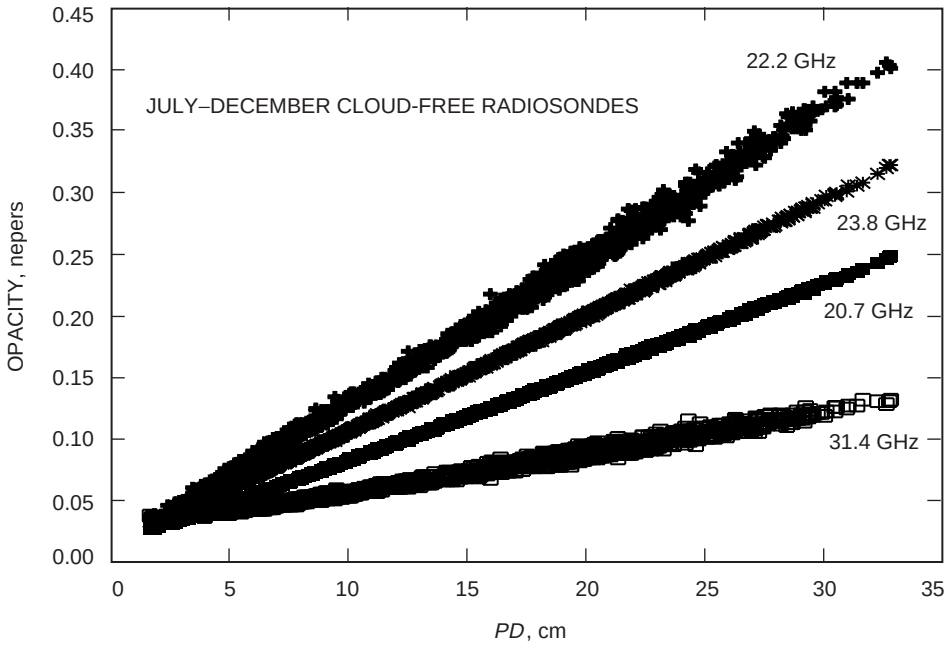

Fig. 2. CART site radiosonde computations of WVR-channel opacities versus wet delay using the JPL vapor absorption model.

CART site. The Liebe–Rosenkranz [29] oxygen and JPL water vapor absorption models were used to compute the opacities. The frequencies shown include all operating channels of WVRs used in this study. The scatter about linear regression fits is due to variations both in atmospheric temperature and in the height distribution of the water vapor. The height distribution (pressure broadening) effect is most pronounced at the 22.2 GHz line center, but is greatly reduced at the 20.7 and 23.8 GHz "hinge" frequencies where the pressure dependencies are minimal. Variations in surface pressure also contribute a small component to the scatter.

Our method for confirming/refining the vapor absorption model is to match modeled and measured values of the τ_ν versus PD regression slope ($=\Delta\tau_\nu/\Delta PD$) at each of the WVR frequencies. This differential approach eliminates the spurious effects of WVR calibration offsets and uncertainties in the assumed oxygen absorption model and minimizes the effects of WVR gain errors and drifts. Table 1 shows these effects on the $\Delta\tau_\nu/\Delta PD$ values computed from the theoretical database shown in Fig. 2 for maximum realistic perturbations of the absorption model and WVR calibration parameters.

Table 1. Sensitivity of the $\Delta\tau_\nu/\Delta PD$ regression slope to absorption model and WVR calibration errors.

Oxygen model	Vapor model	WVR calibration	$\Delta\tau_\nu/\Delta PD$, nepers/cm				Change from nominal, percent			
			20.7 GHz	22.2 GHz	23.8 GHz	31.4 GHz	20.7 GHz	22.2 GHz	23.8 GHz	31.4 GHz
Nominal	Nominal	Perfect	0.00711	0.01178	0.00931	0.00316	—	—	—	—
Nominal	0.9 × nominal	Perfect	0.00640	0.01059	0.00837	0.00283	−10.0	−10.1	−10.3	−10.4
0.84 × nominal	Nominal	Perfect	0.00712	0.01179	0.00932	0.00318	0.1	0.1	0.1	0.6
Nominal	Nominal	+1 K offset	0.00713	0.01182	0.00933	0.00316	0.3	0.3	0.2	0.0
Nominal	Nominal	+1 percent gain	0.00708	0.01175	0.00928	0.00312	−0.4	−0.3	−0.3	−1.3

Note that the only plausible parameter that can produce a significant variation in the $\Delta\tau_\nu/\Delta PD$ determination for the archive is the vapor absorption strength. As expected, plausible offset effects, either in the WVR calibration or the assumed strength of the oxygen model, produce <1 percent variation in the regression slope parameter. Note also that the 1 percent assumed gain error shown in Table 1 far exceeds the gain errors (0.2 to 0.3 percent) expected from the WVR tip-curve calibrations described in Section IV.

For actual WVR-derived opacity and GPS-derived PD measurements, a large volume of data, spanning a large fraction of the realizable range of humidity conditions, is required to constrain the $\Delta\tau_\nu/\Delta PD$ parameter to the 2 to 3 percent accuracy level. Effects such as temperature variations, vapor height distribution, and pressure broadening, which contribute to the scatter illustrated in Fig. 2, must be minimized by averaging over a wide range of conditions. The interpretation of the regression slope parameter in terms of an optimum vapor absorption model is accomplished by comparisons with model-generated slopes derived from site- and season-specific radiosonde data. For a radiosonde archive representative of the experiment conditions, absorption models are evaluated according to their $\Delta\tau_\nu/\Delta PD$ prediction relative to the actual $\Delta\tau_\nu/\Delta PD$ measurements derived from the GPS and WVR data. Although the modeled database always consists of radiosonde computations, the radiosonde accuracy is not critical to our results. No specific radiosonde is being compared individually with either WVR or GPS data products.

The radiosondes are used only to predict the expected $\Delta\tau_\nu/\Delta PD$ value for different absorption models and a specific site and season. Thus, what is critical is that the radiosonde archive provide a statistically representative sampling of the pressure, temperature, and humidity conditions encountered during the WVR–GPS comparison measurements. The uncertainty in these radiosonde-based model predictions of the $\Delta\tau_\nu/\Delta PD$ parameter varies with frequency and is evaluated in Section V.

IV. WVR–GPS Comparison Data Sets and Processing

Collocated WVR and GPS data were obtained continuously for a 2 month duration at the Goldstone tracking station (GTS) in the Mojave Desert from August 28 through October 25, 1997, and for a 3 month duration at the Lamont, Oklahoma, CART site from July 2 through September 25, 1998. Both sites were also equipped with a surface meteorological station (measurements of surface temperature, pressure, and humidity) and a microwave temperature profiler (MTP) to provide additional constraints on the atmospheric conditions during the WVR–GPS campaigns.

GPS carrier phase and pseudorange data (every 30 seconds) were processed in 24 hour batches using the GIPSY/OASIS II software [30] and holding the ephemerides and clocks fixed to the values provided by the JPL International GPS Service (IGS) Analysis Center.[7] Following [21], data from all available GPS satellites with elevation angles above 7 deg were processed (5 to 12 satellites). The zenith wet delay was treated as a random walk process, which accumulates 9 mm of variance every hour. The Niell mapping function [26] was used to model the elevation dependence of the wet and dry components of the tropospheric delay. Tropospheric delay gradients were treated as a random walk process with accumulations of 0.09 mm/h [21]. The stochastic zenith delay estimates (wet plus dry) were output every 5 minutes. Wet delays were then obtained by subtraction of the dry component, derived from surface pressure measurements [22]. Combinations of hardware failures and flagged questionable data eliminated approximately 50 percent of the potential GPS data at the Goldstone site, leaving 8,425 5-minute-interval wet delay measurements. At the Oklahoma CART site, GPS data outage totaled 27 percent, leaving 15,228 wet delay measurements.

WVR zenith brightness temperatures were obtained from two independent instruments at Goldstone and three independent instruments at the Oklahoma CART site. Individual descriptions are provided below. For all five instruments, absolute calibration was based on tip-curve measurements that typically produce 0.5 to 1.0 K absolute accuracy in brightness temperature under clear (cloud-free) conditions [31]. WVR zenith brightness temperature sampling intervals ranged from 5 seconds to 2 minutes, depending on the instrument. Hardware failures occurred infrequently, yielding at least 80 percent experiment coverage for all five WVRs. For analysis purposes, all WVR brightness temperature measurements were converted to opacities [Eq. (5)], then merged with the GPS wet delay measurements by averaging the WVR data over a 5 minute interval centered on each GPS time tag.

A. Goldstone J03 WVR Data

The JPL J03 WVR [32] measures sky radiation at three frequencies: 20.7, 22.2, and 31.4 GHz. At Goldstone, the instrument operated in a continuous tip-curve mode that provided calibration data and zenith brightness temperatures at 3 minute intervals. By operating in the continuous tip-curve mode, gain fluctuations due to instrument temperature variations were continuously monitored, maintaining approximately 1 K absolute calibration accuracy for each clear-sky tip curve. Tip curves that did not satisfy a quality of fit criterion (<1 K rms for each channel) were removed from the database, effectively eliminating most cloudy conditions and other anomalous effects. The effects of lateral inhomogeneities in the tropospheric water vapor distribution can be removed by smoothing tip-curve results, effectively reducing the calibration uncertainty to approximately 0.5 K. However, the J03 brightness temperature data utilized in the current study were obtained without tip-curve smoothing, instead relying on the large

[7] ftp://sideshow/pub/jpligsac.

volume of data (approximately 16,000 independent zenith brightness temperature measurements over the 2 month Goldstone experiment) to average out stochastic effects. The correlation of the J03-measured zenith opacities with the GPS-derived wet delays for the 1997 Goldstone experiment is shown in Fig. 3.

B. Goldstone R06 WVR Data

The JPL R06 WVR [33] has two channels—20.7 and 31.4 GHz—and requires 4 minutes to complete a tip-curve sequence. The R06 operating mode was also continuous tip curves, each providing two zenith brightness temperature measurements over a 4 minute interval. Instrument gain values used to determine zenith brightness temperatures were smoothed using a linear relationship between gain and mixer temperature obtained from the previous 24 hours of calibration data. The resultant brightness temperature accuracy is estimated to be 0.5 K for clear conditions. A two-channel cloud-liquid retrieval algorithm was applied to the brightness temperatures to remove cloudy condition data, leaving approximately 17,000 measurements over the experiment interval. The correlation of the R06-derived opacities with the Goldstone GPS-derived wet delays is shown in Fig. 4.

C. Oklahoma CART Site J02 WVR Data

The JPL J02 WVR is essentially a duplicate of the J03 instrument deployed at Goldstone, operating at 20.7, 22.2, and 31.4 GHz in the continuous tip-curve mode throughout the 3 month CART site experiment. The zenith brightness temperatures were extracted from individual tip-curve measurements that passed a "quality of tip-curve fit" criterion, eliminating most of the cloudy and otherwise anomalous data. No smoothing of the brightness temperature data was performed prior to merging with the GPS wet delay data at the GPS 5 minute time tags. Approximately 30,000 high quality J02 data records were obtained over the July through September 1998 CART site experiment interval. For clarity, only the August 1998 comparison data between J02-derived opacities and GPS-derived wet delays are shown in Fig. 5. The full range of wet delays seen at the CART site ranged from 5 cm (observed in September 1998) to 35 cm (observed in July 1998).

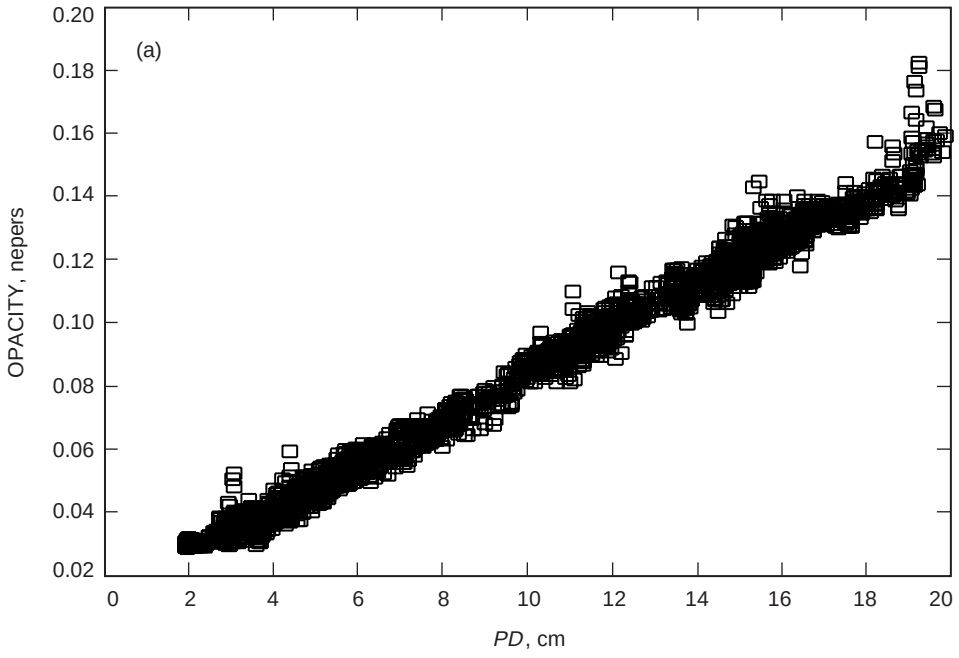

Fig. 3. Measurements of J03 WVR-derived opacities versus GPS-derived wet path delay at the Goldstone site: (a) 20.7 GHz channel, (b) 22.2 GHz channel, and (c) 31.4 GHz channel.

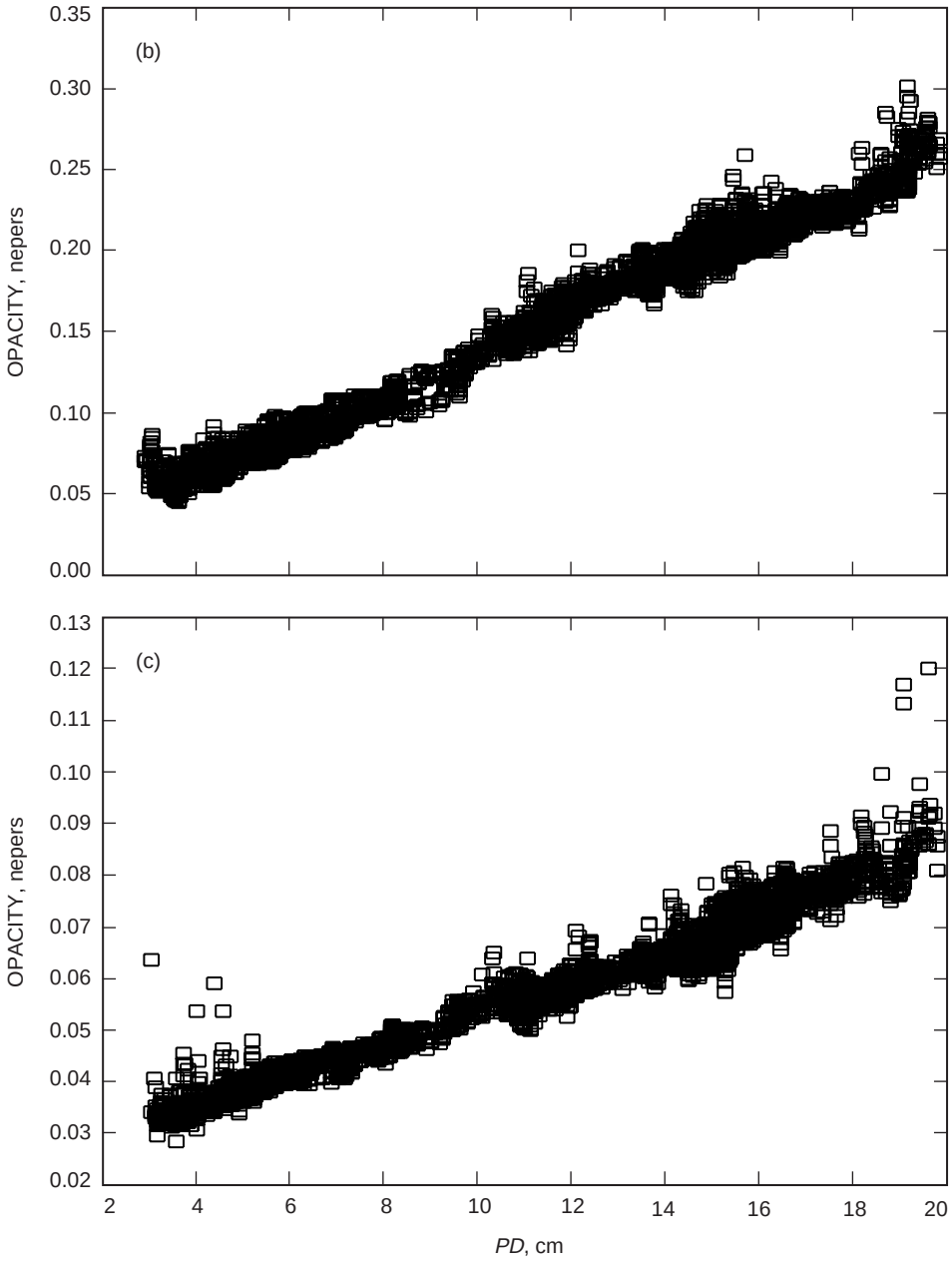

Fig. 3 (cont'd).

D. Oklahoma CART Site D02 Data

The JPL D02 WVR[8] operates at the same frequencies as the R06 unit (20.7 and 31.4 GHz) but has a significantly different mechanical design. It also was operated in a continuous tip-curve mode for the CART site experiment duration, yielding independently calibrated brightness temperature measurements at 2.5 minute intervals. The quality-of-fit tip-curve criterion was applied to eliminate cloudy and anomalous data, leaving approximately 48,000 brightness temperature records over the 3 month experiment. No smoothing of the data was performed prior to merging with the GPS data archive. The D02-derived opacities are shown versus the August 1998 GPS-derived wet delays in Fig. 6.

[8] S. J. Keihm, B. L. Gary, and S. J. Walter, *Spain 31 GHz Observations of Sky Brightness Temperatures: June 1990–June 1992*, JPL D-10710 (internal document), Jet Propulsion Laboratory, Pasadena, California, October, 1992.

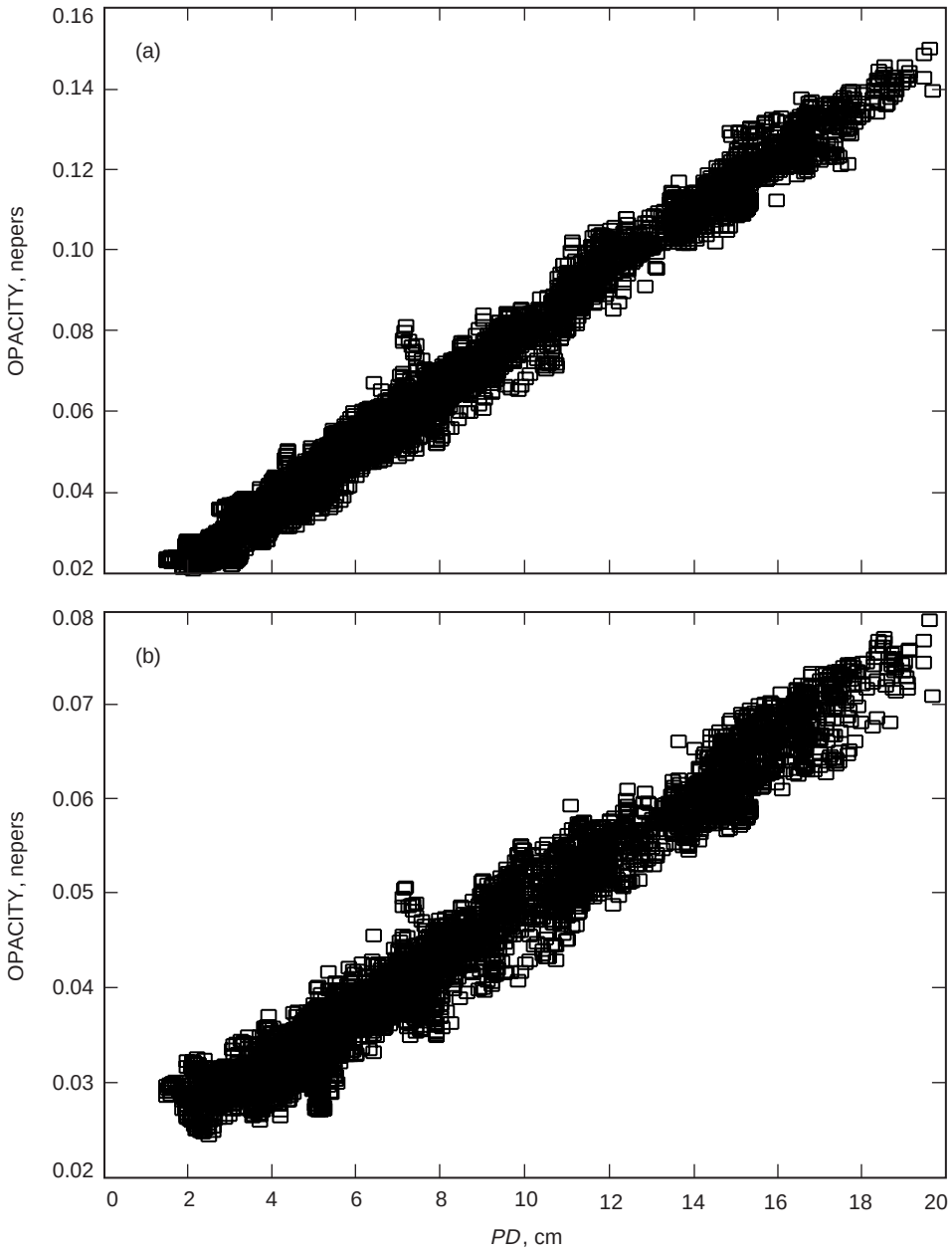

Fig. 4. Measurements of R06 WVR-derived opacities versus GPS-derived wet path delay at the Goldstone site: (a) 20.7 GHz channel and (b) 31.4 GHz channel.

E. Oklahoma CART Site Microwave Water Vapor Radiometer (MWR) Data

The MWR unit [34] is a dual-frequency WVR permanently deployed by the U.S. Department of Energy Atmospheric Radiation Measurement Program at the Oklahoma CART site. It measures atmospheric brightness temperatures at 23.8 and 31.4 GHz. During most of the July through September 1998 time frame, the MWR unit obtained zenith brightness temperature measurements at 20 second intervals, accumulating approximately 240,000 data records. Tip-curve calibrations were performed monthly with gain variations monitored using noise diodes. The data were not filtered for cloudy conditions, reflected in the scatter shown in the MWR-derived opacity versus GPS-derived wet delay plot of Fig. 7. As explained below, the cloudy cases are effectively removed as outliers in the subsequent regression fits of opacity versus wet delay.

V. Regression Analysis and Vapor Absorption Model Constraints

A. Model Predictions of Site, Season, and Annual Variability of $\Delta\tau_V / \Delta PD$

We propose that the $\Delta\tau_\nu/\Delta PD$ regression slopes derived from data such as those shown in Figs. 3 through 7 provide a meaningful constraint on the 20 to 32 GHz atmospheric vapor absorption model, largely independent of plausible GPS scale errors, WVR calibration errors, and oxygen absorption model uncertainties. The regression slopes depend almost entirely on the vapor absorption strength, with small secondary effects specific to site and season. The magnitudes of the site and seasonal effects on the

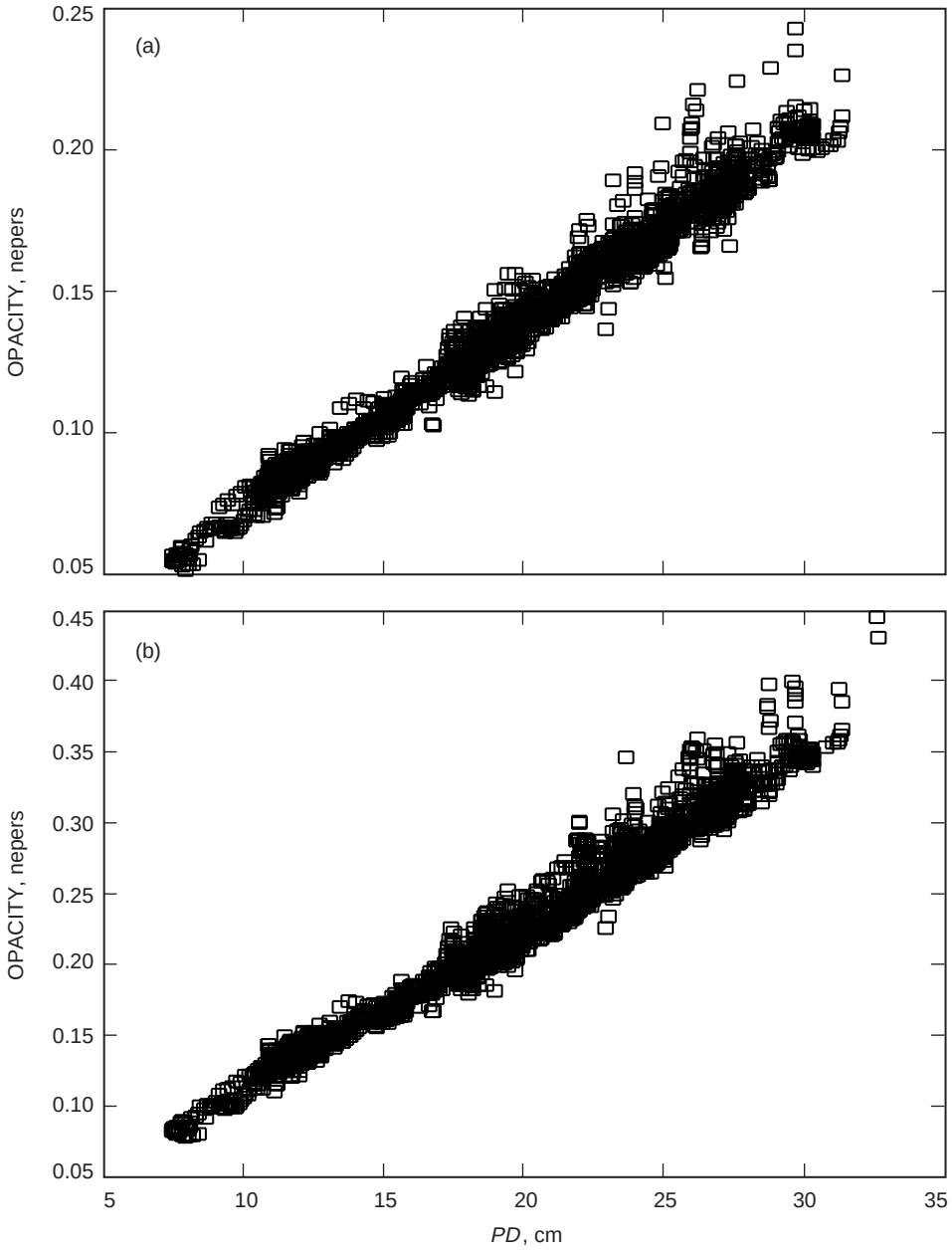

Fig. 5. Measurements of J02 WVR-derived opacities versus GPS-derived wet path delay at the CART site: (a) 20.7 GHz channel, (b) 22.2 GHz channel, and (c) 31.4 GHz channel.

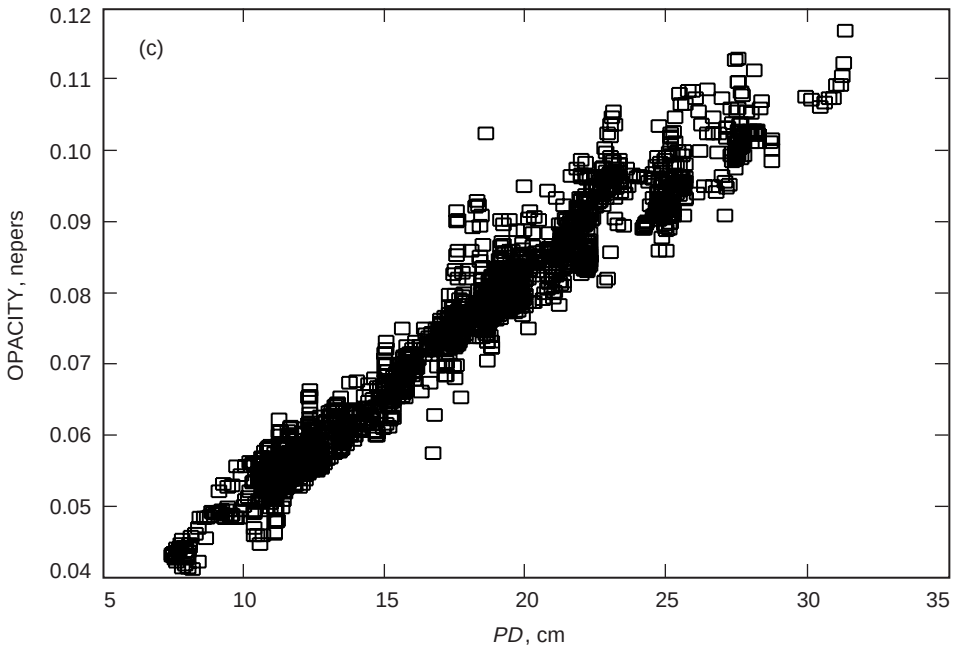

Fig. 5 (cont'd).

$\Delta\tau_\nu/\Delta PD$ parameter for the Goldstone and CART site environments are illustrated in Table 2, derived from regression fits to τ_ν, PD data pairs obtained from radiosonde calculations using the JPL absorption model.

The CART site radiosonde facility is within 100 m of all the WVR and GPS instrumentation utilized at that site for this study. The Desert Rock, Nevada, radiosonde site, with comparable elevation and similar climatology, serves as a proxy for the Goldstone experiment site, which is not a location of radiosonde launches. For all Desert Rock radiosonde calculations, surface pressure values were adjusted downward by 8 mb to account for the mean surface pressure difference between Desert Rock and Goldstone Deep Space Station (DSS) 13. The adjusted pressure profile was then computed from hydrostatic equilibrium using the temperature and humidity profile provided by the radiosonde. The CART archive includes the July through December months for the years 1995 through 1999, totaling 1863 clear radiosondes. The Desert Rock archive includes full-year coverage for the interval from 1980 through 1988, totaling 4573 clear radiosondes. The July through September (914 clear radiosondes) and September through October (799 clear radiosondes) included-month intervals, shown in Table 2, correspond to the GPS–WVR experiment durations at the CART and GTS sites. The $\Delta\tau_\nu/\Delta PD$ regression slope values were computed from all available years for the specified months using the JPL absorption model.

Note in Table 2 the contrast between the season and site variability of $\Delta\tau_\nu/\Delta PD$ in the WVR channels. At 20.7 and 23.8 GHz, the $\Delta\tau_\nu/\Delta PD$ parameter varies less than 1 percent with season (included months) and site. At 22.2 and 31.4 GHz, however, the site differences in the regression slopes are significantly larger, primarily due to the elevation (mean surface pressure) difference between the CART site and Desert Rock. Due to pressure broadening of the 22.2 GHz spectral line, the vapor absorption coefficient increases with decreasing pressure at the line center, and decreases with decreasing pressure in the far wing of the line at 31.4 GHz. At the 20.7 and 23.8 GHz hinge frequencies, the pressure dependence of absorption is near minimum—thus the absence of $\Delta\tau_\nu/\Delta PD$ dependence on site elevation. The larger seasonal differences at 22.2 and 31.4 GHz also may be due to the pressure broadening effect, but would require a seasonal shift in the local height distribution of the water vapor since there is no significant seasonal variation in the mean surface pressures.

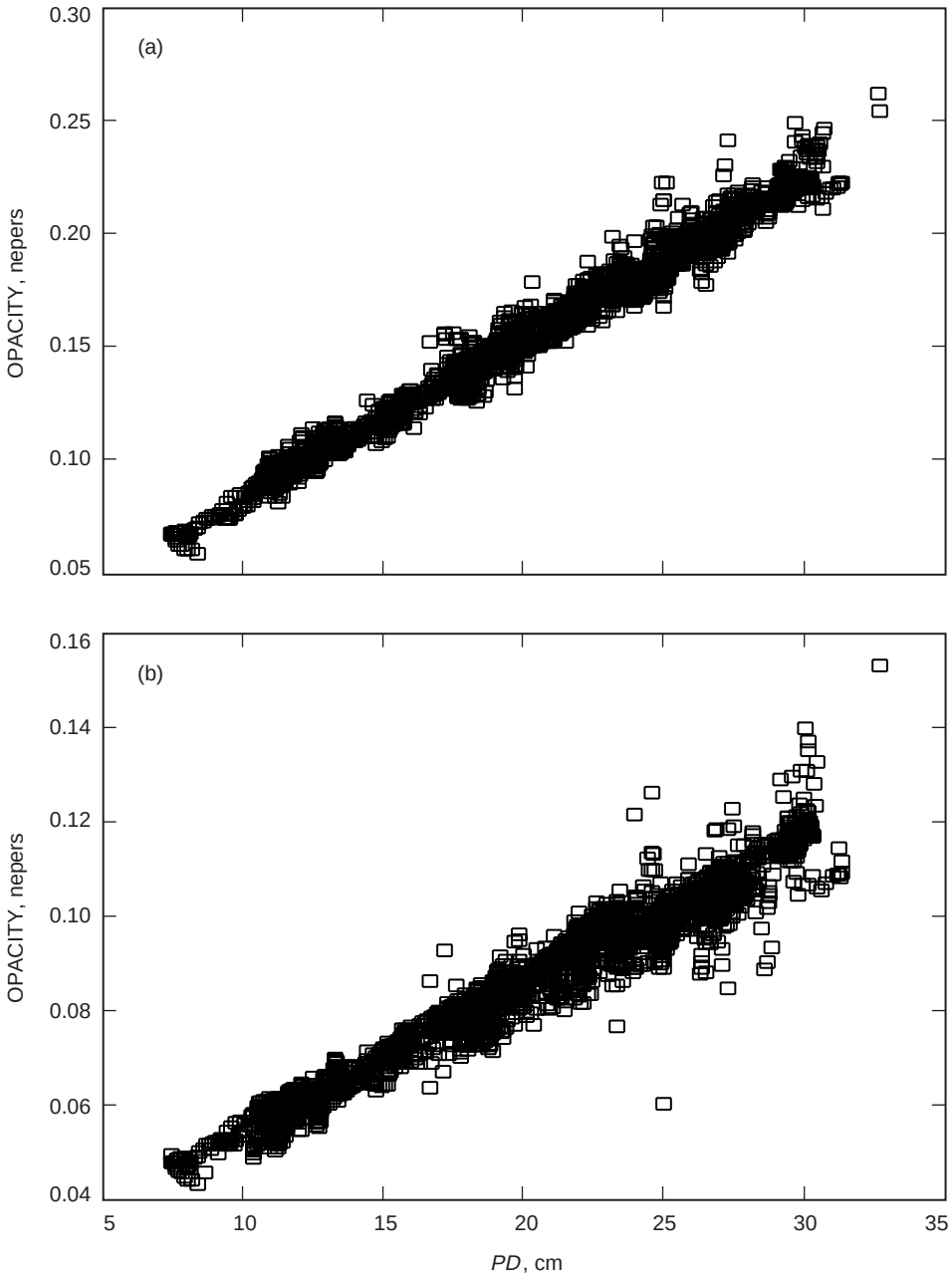

Fig. 6. Measurements of D02 WVR-derived opacities versus GPS-derived wet path delay at the CART site: (a) 20.7 GHz channel and (b) 31.4 GHz channel.

The annual variability column of Table 2 gives the standard deviation (in percent) of the calculated regression slopes for individual calendar years included at each site (i.e., the variability between the regression slopes for different years). Note the contrasts between the 20.7 and 23.8 GHz hinge channels (<0.5 percent year-to-year variability) and the 22.2 and 31.4 GHz channels (up to 4 percent annual variability for the summer-month intervals). These values are representative of the uncertainties inherent in the $\Delta\tau_\nu/\Delta PD$ predictions for any of the candidate absorption models for the specified sites and month intervals, and, therefore, are indicative of the accuracy limitations that can be claimed for absorption model constraints derived from the current GPS–WVR measurements of $\Delta\tau_\nu/\Delta PD$.

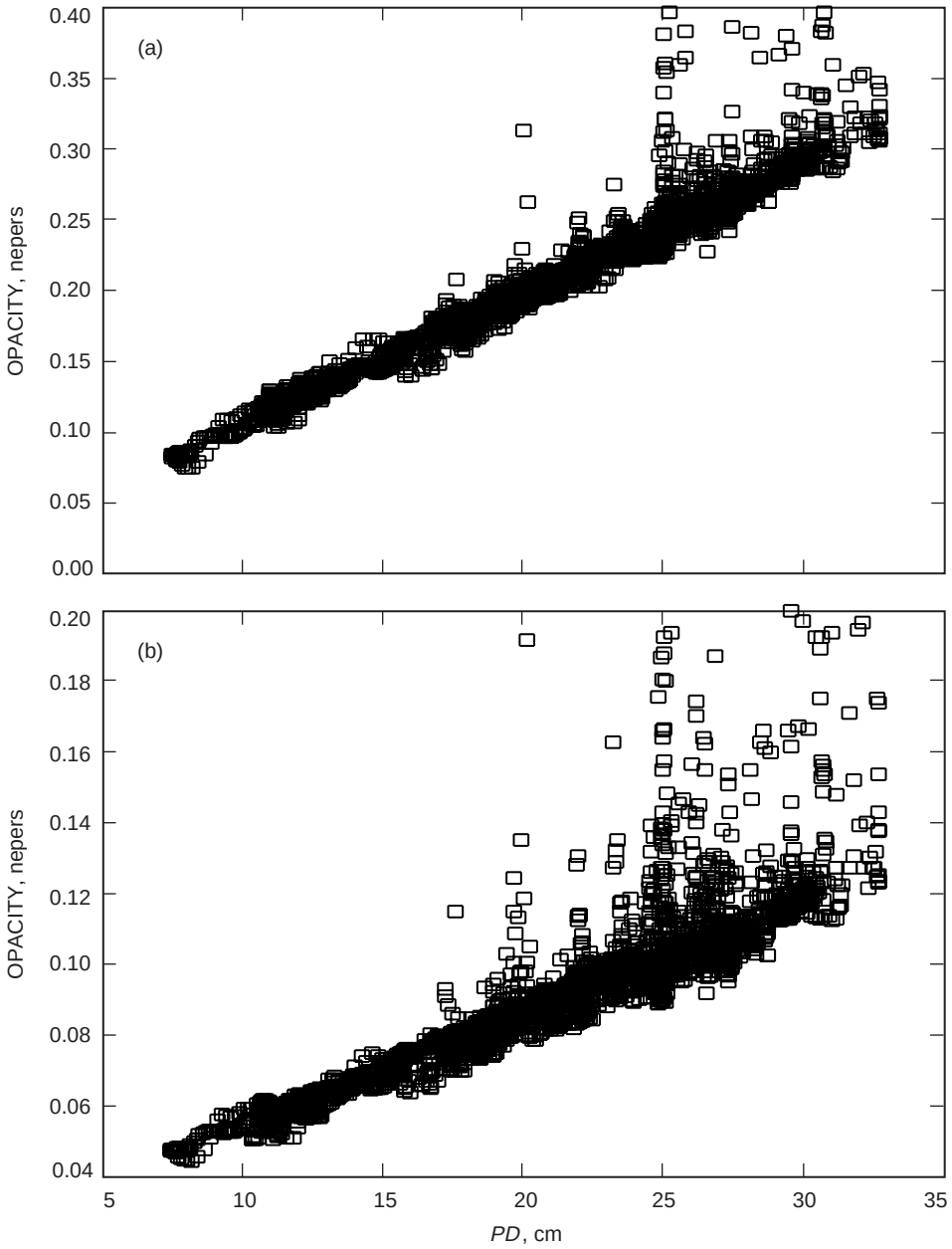

Fig. 7. Measurements of MWR-derived opacities versus GPS-derived wet path delay at the CART site: (a) 23.8 GHz channel and (b) 31.4 GHz channel.

We also have examined the sensitivity of the model predictions to the restricted local time sampling of the radiosondes, which typically are launched twice daily at 0 and 1200 UT. The concern is that unsampled diurnal effects could lead to significant errors in the radiosonde-based model predictions of the $\Delta\tau_\nu/\Delta PD$ parameter when compared with the GPS–WVR measurements which uniformly sample the full diurnal cycle. Regression slope calculations were performed for subsets of the radiosonde-based model predictions using the 0 UT and 1200 UT data separately for the month intervals corresponding to the GPS–WVR measurements. For the Desert Rock radiosondes, the largest 0 UT or 1200 UT difference relative to the complete archive result was 1.5 percent, occurring for the 31.4 GHz predictions. At all other channels, the differences were less than 0.6 percent. For the CART site radiosondes, all 0 UT or 1200 UT differences were less than 0.4 percent. We therefore dismiss local time biasing as a significant source of model prediction error for the $\Delta\tau_\nu/\Delta PD$ parameter.

Table 2. Model predictions of the dependence of the $\Delta\tau_\nu / \Delta PD$ regression slope parameter on site and season, computed from radiosondes using the JPL vapor absorption model.[a]

Raob site	Years	Included months	$\overline{Ts}$, K	$\overline{Ps}$, mb	$\overline{PD}$, cm	Frequency, GHz	$\Delta\tau_\nu/\Delta PD$, nepers/cm	Annual variability, percent
CART	1995–1999	July–December	295.0	978.7	15.0	20.7	0.00711	0.1
						22.2	0.01172	0.6
						23.8	0.00930	0.1
						31.4	0.00317	1.2
CART	1995–1999	July–September	301.7	977.1	20.4	20.7	0.00717	0.4
						22.2	0.01212	3.5
						23.8	0.00937	0.4
						31.4	0.00328	4.3
Desert Rock	1980–1988	January–December	291.0	899.8	7.8	20.7	0.00713	0.2
						22.2	0.01292	0.6
						23.8	0.00932	0.2
						31.4	0.00257	3.2
Desert Rock	1980–1988	September–October	296.7	900.0	9.4	20.7	0.00713	0.4
						22.7	0.01272	1.1
						23.8	0.00931	0.5
						31.4	0.00271	4.6

[a] The columns headed $\overline{Ts}$, $\overline{Ps}$, and $\overline{PD}$ specify the mean values of surface temperature, surface pressure, and wet delay determined from the radiosonde archive specified by the three left-most columns.

B. WVR–GPS Measurements of $\Delta\tau_\nu / \Delta PD$ and Comparisons with Models

The measured $\Delta\tau_\nu/\Delta PD$ values, derived from the data illustrated in Figs. 3 through 7, were obtained by iterative linear regression fits. After each regression, the rms of the residuals was computed and used as a criterion for removing outlier data. The regressions were repeated after eliminating all data that deviated from the previous linear fit by more than twice the residual rms. The process was repeated until no outliers resulted. The iterative fit process typically eliminated 20 percent of the original archive and ensured the removal of marginal data, including light cloud conditions and the occurrence of condensation on the reflectors or radome covers of the WVRs. Table 3 gives the regression results for $\Delta\tau_\nu/\Delta PD$ for each of the WVR channels at the CART and Goldstone sites. Also shown are the model predicted slope values for the JPL, Cruz, and Liebe87 absorption models. The CART site model predictions were derived from the July through September 1998 radiosonde data, obtained from the launch facility collocated with the GPS–WVR instrumentation. The Goldstone model predictions were derived from the elevation-adjusted Desert Rock radiosonde data obtained from the September through October subset of the entire 1980 through 1988 archive.

Note first the degree of consistency for common WVR channels and sites in the measured $\Delta\tau_\nu/\Delta PD$ column of Table 3. At 20.7 GHz, the difference in measured $\Delta\tau_\nu/\Delta PD$ is 2.6 percent at the CART site (J02 and D02) and 1.7 percent at Goldstone (J03 and R06). At 31.4 GHz, the variation is 3.7 percent at the CART site (J02, D02, and MWR) and 3.2 percent at Goldstone (J03 and R06). This result, including independent data from five different radiometers, provides evidence that the $\Delta\tau_\nu/\Delta PD$ parameter can constrain the vapor absorption model to the 3 percent level. In the comparisons with model-generated $\Delta\tau_\nu/\Delta PD$ values, however, uncertainties in the representativeness of the radiosonde

Table 3. Measurement–model comparisons of the $\Delta\tau_\nu / \Delta PD$ parameter.

Site	Frequency, GHz	WVR	Measured $\Delta\tau/\Delta PD$, nepers/cm	Model-predicted $\Delta\tau_\nu/\Delta Pd$ and the difference from measured values					
				JPL model	Difference, percent	Cruz model	Difference, percent	Liebe model	Difference, percent
Cart	20.7	J02	0.00684	0.00715	+4.5	0.00705	+3.1	0.00679	−0.7
Cart	20.7	D02	0.00702	0.00715	+1.9	0.00705	+0.4	0.00679	−3.3
GTS	20.7	J03	0.00707	0.00713	+0.8	0.00706	−0.1	0.00677	−4.2
GTS	20.7	R06	0.00719	0.00713	−0.8	0.00706	−1.8	0.00677	−5.8
Cart	22.2	J02	0.01183	0.01222	+3.3	0.01162	−1.8	0.01161	−1.9
GTS	22.2	J03	0.01232	0.01272	+3.2	0.01209	−1.9	0.01208	−1.9
Cart	23.8	MWR	0.00904	0.00935	+3.4	0.00922	+2.0	0.00887	−1.9
Cart	31.4	J02	0.00332	0.00330	−0.6	0.00330	−0.6	0.00309	−6.9
Cart	31.4	D02	0.00320	0.00330	+3.1	0.00330	+3.1	0.00309	−3.4
Cart	31.4	MWR	0.00323	0.00330	+2.2	0.00330	+2.2	0.00309	−4.3
GTS	31.4	J03	0.00272	0.00271	−0.4	0.00272	0.0	0.00253	−7.0
GTS	31.4	R06	0.00281	0.00271	−3.6	0.00272	−3.2	0.00253	−10.0

archive also must be considered. This uncertainty is reflected in the annual variability column of Table 2 and is clearly more important for the 22.2 and 31.4 channels, which are most sensitive to the pressure-broadening effect.

Inspection of the percentage of difference columns in Table 3 reveals the models' performances relative to the individual channel measurements. Comparing the model predictions with the measured $\Delta\tau_\nu/\Delta PD$ values for each site–frequency combination, we find that the Cruz model errors lie within the range from −3.2 percent to +3.1 percent for all four sampled frequencies. The JPL absorption model appears to be from 3 to 4 percent too high for the CART site conditions at the three lower channels most sensitive to the 22.2 GHz absorption feature. The Liebe87 model appears to be low at all channels, by 2 to 10 percent for the Goldstone site conditions. The Liebe87 model discrepancy is largest at 31.4 GHz, suggesting that this model underestimates the continuum contribution by 4 to 10 percent.

In order to properly assess the significance of the model-predicted versus measured differences shown in Table 3, we have averaged the regression slopes measured by different WVRs for common site–frequency combinations and estimated uncertainties in both the measured and model-generated $\Delta\tau_\nu/\Delta PD$ values. The results are presented in Table 4. The measurement uncertainties, shown as ± percent values in the fourth column, are derived from two factors. The first reflects the measured variation about the mean when more than one WVR was available for a specific site–channel combination. The second factor is based on an evaluation of the error due to sampling bias. This component of the measurement uncertainty was estimated by splitting the database for each WVR channel into odd and even days, and then recomputing the $\Delta\tau_\nu/\Delta PD$ values for each data subset. The uncertainties shown in the fourth column of Table 4 represent one-half of the maximum peak-to-peak variations in computed regression slopes due to the two factors described above. The formal statistical uncertainties of the regression slope determinations were negligible (<0.3 percent) in all cases.

In addition to the measurement errors, the uncertainties in the model-predicted $\Delta\tau_\nu/\Delta PD$ values, shown in the far right column of Table 4, limit the accuracy with which we can constrain the vapor

Table 4. Measurement–model comparisons and error estimates of the $\Delta\tau_V / \Delta PD$ slope parameter after averaging common site–channel combinations.

Site	Frequency, GHz	WVRs used	WVR-averaged $\Delta\tau_\nu/\Delta PD$, nepres/cm ± percent	Model differences versus measured values, percent			Model uncertainty, percent
				JPL	Cruz	Liebe87	
Cart	20.7	J02, D02	0.00693 ± 2.1	+3.2	+1.7	−2.0	0.4
GTS	20.7	J03, R06	0.00713 ± 1.2	0.0	−1.0	−5.0	0.4
Cart	22.2	J02	0.01183 ± 1.6	+3.3	−1.8	−1.9	3.5
GTS	22.2	J03	0.01232 ± 2.2	+3.2	−1.9	−1.9	1.1
Cart	23.8	MWR	0.00904 ± 0.7	+3.4	+2.0	−1.9	0.4
Cart	31.4	J02,D02, MWR	0.00325 ± 3.2	+1.5	+1.5	−4.9	4.3
GTS	31.4	J03, R06	0.00277 ± 3.3	−2.0	−1.6	−8.5	4.6

absorption model from the GPS–WVR comparison data. The model uncertainty values are obtained from the annual variability column of Table 2 and reflect the year-to-year variability of the regression slopes computed from radiosonde data. The uncertainty values are probably overly conservative for the CART site in that the model predictions are based on collocated radiosondes obtained over the same time interval (July through September 1998) as the WVR–GPS measurements. However, the July through September 1998 CART site archive included only 101 radiosondes, and formal statistical uncertainties in the regression slopes were in the 1 to 2 percent range for the 22.2 and 31.4 GHz channels. These values may be more representative of the uncertainties in the CART site model predictions of regression slopes.

The model difference results in Table 4 indicate that the Cruz model provides the best overall fit to the GPS–WVR $\Delta\tau_\nu/\Delta PD$ measurements for the combined site data, with model-minus-measurement differences of 2.0 percent or less at all channels. The Cruz model differences lie well within the combined uncertainties due to the derived measurement and model-prediction errors for all site–channel combinations with the exception of the CART site 23.8 GHz channel. Note, however, that the measurement uncertainty for this channel likely is underestimated since instrument-to-instrument variability was not included in the error estimate (with only one WVR operating at 23.8 GHz).

The JPL vapor absorption model appears to be 3 percent high, exceeding the measurement uncertainties, at the primary vapor-sensing channels (20.7, 22.2, and 23.8 GHz), with the exception of the Goldstone 20.7 GHz comparison. The Liebe87 model yields small differences relative to the measurements, comparable in magnitude to the Cruz model, at the primary vapor-sensing channels, with the exception of the Goldstone 20.7 GHz comparison. At 31.4 GHz, the Liebe model appears to be from 5 to 8 percent too low, depending on the site, with the differences from measurements exceeding even the largest measurement uncertainties.

Based on the Table 4 results, it appears that the Cruz vapor absorption model meets the accuracy requirements of the Cassini GWE tropospheric calibration system at Goldstone. Small revisions in model parameters could be made to further reduce the Cruz model differences at the GTS site. However, such refinements are not warranted in view of the current measurement and model-prediction uncertainties. We therefore recommend that the Cruz model, as formulated in the Appendix (with $C_L = 1.064$, $C_W = 1.066$, and $C_C = 1.237$), be utilized in the generation of future Goldstone algorithms for the estimation of tropospheric water-vapor-related parameters from 20 to 32 GHz radiometric measurements.

VI. Summary and Recommendations

Comparisons of WVR-derived opacities with collocated GPS-derived wet path delays have been analyzed to constrain the atmospheric water vapor absorption model over the 20 to 32 GHz spectral band. A differential approach, utilizing the fitted regression slope ($\Delta\tau_\nu/\Delta PD$) of opacity-versus-path delay data, provides an absorption model metric that is insensitive to oxygen model uncertainties and plausible WVR calibration errors. A total of 5 months of 5-minute-interval data from the Oklahoma CART site and the Goldstone, California, tracking station provided a sufficiently large database to span the full ranges of humidity conditions at both locations.

Data using five independently calibrated WVRs demonstrated consistency at the 2 to 3 percent level for the measured $\Delta\tau_\nu/\Delta PD$ slope values at four WVR frequencies. Comparisons with three candidate model-derived $\Delta\tau_\nu/\Delta PD$ slope values suggest that the Cruz model best fits the combined data from both sites, with model-minus-measurement differences of ± 2 percent over the 20 to 32 GHz range. The JPL model comparisons with the measurements are only slightly inferior to the Cruz model results, with an apparent +3 percent bias in the 20 to 24 GHz vapor-sensing band. We note, however, that these differences are comparable to the combined uncertainties of the measurements and model predictions. With the exception of the Goldstone site 20.7 GHz channel, the Liebe87 model produces 2 percent agreement with the 20 to 24 GHz measurements. The largest measurement-model differences seen in all of the data occurred for the Liebe87 predictions of the 31.4 GHz $\Delta\tau_\nu/\Delta PD$ parameter, with the data indicating that the Liebe87 model underestimates the continuum component of vapor absorption by 5 to 8 percent.

The accuracy of the opacity-versus-path delay regression slope as an absorption model constraint is limited primarily by uncertainties in the radiosonde-based model predictions of $\Delta\tau_\nu/\Delta PD$. The errors are due to variations in the radiosonde samplings of the relative height distribution of the water vapor. At the 22.2 and 31.4 GHz frequencies, most sensitive to pressure-broadening effects, the $\Delta\tau_\nu/\Delta PD$ predictions are characterized by up to 4 percent inter-annual variability. The model prediction uncertainty is much less at the 20.7 and 23.8 GHz hinge frequencies, the primary vapor-sensing channels in most ground-based water vapor radiometers. Thus, it can be argued that vapor burden and wet path delay measurements, provided by well-calibrated WVRs operating at either of these frequencies, can be obtained with 2 to 3 percent accuracy if the Cruz model is used in the retrieval algorithm generation. The 2 to 3 percent accuracy estimate meets the GWE tropospheric calibration system requirements and represents a marked improvement over the 5 to 10 percent model uncertainties associated with the radiosonde-derived constraints of the past.

It is recommended that the Cruz absorption model be adopted for the generation of future algorithms for the WVR-based estimation of wet path delay at Goldstone, in particular for the tropospheric calibration system now being implemented to support the Cassini GWE and other radio science experiments. The principal instrument of this path delay calibration system is an advanced, three-channel water vapor radiometer (AWVR) operating at 22.2, 23.8, and 31.4 GHz. We also recommend that a new comparison data set be generated between GPS-derived wet delays and AWVR-derived opacities at Goldstone during winter-month conditions. The goal will be to obtain tighter absorption model constraints for all AWVR channels during Goldstone climatic conditions representative of the expected GWE environment. Unlike the 1997 Goldstone GPS–WVR experiment, the comparisons will include the 23.8 GHz channel, a critical observable for the GWE tropospheric calibration system. If undertaken at DSS 25, the site of the Cassini tracking station, the experiment could also utilize data from the redundant calibration system (two identical side-by-side AWVRs), allowing a more precise estimate of the instrument error component of the $\Delta\tau_\nu/\Delta PD$ measurements.

Acknowledgments

Gabriel Garcia-Jordan and Allen Hubbard of the Microwave, Lidar, and Interferometer Section refurbished the WVR hardware prior to field operations and conducted the CART site deployment. Martin Marcin of the Tracking Systems and Applications Section conducted field operations for the JPL GPS receiver deployed at the CART site and assisted in the data acquisition. Invaluable support from the CART site personnel, led by site manager James Teske, proved critical throughout the July through September 1998 experiment period. Roger Linfield, Allan Tanner, and George Resch provided incisive comments and many useful recommendations in their reviews of preliminary drafts of this article.

References

[1] G. Elgered, "Tropospheric Radio Path Delay from Ground-Based Microwave Radiometry," Chapter 5 in *Atmospheric Remote Sensing by Microwave Radiometry*, edited by M. A. Janssen, New York: Wiley, 1993.

[2] S. J. Keihm, M. A. Janssen, and C. S. Ruf, "TOPEX/Poseidon Microwave Radiometer (TMR): III. Wet Troposphere Range Correction Algorithm and Prelaunch Error Budget," *IEEE Trans. Geosci. Rem. Sensing*, vol. 33, no. 1, pp. 147–161, 1995.

[3] G. M. Resch, Y. Bar-Sever, S. J. Keihm, P. Kroger, R. P. Linfield, M. J. Mahoney, A. Tanner, and L. P. Teitelbaum, "Atmospheric Calibration for Precision Doppler Tracking of Spacecraft," *Planet. Space Sci.*, vol. 46, no. 9/10, pp. 1257–1261, 1998.

[4] M. Tinto and J. W. Armstrong, "Spacecraft Doppler Tracking as a Narrow-Band Detector of Gravitational Radiation," *Phys. Rev. D*, vol. 58, 042002, 1998.

[5] A. Tanner, "Development of a High Stability Water Vapor Radiometer," *Radio Sci.*, vol. 33, no. 2, pp. 449–462, 1998.

[6] J. W. Waters, "Absorption and Emission by Atmospheric Gases," in *Methods of Experimental Physics*, edited by M. L. Meeks, vol. 12B, New York: Academic Press, pp. 142–176, 1976.

[7] H. J. Liebe, "An Update Model for Millimeter Wave Propagation in Moist Air," *Radio Sci.*, vol. 20, pp. 1069–1089, 1985.

[8] H. J. Liebe and D. H. Layton, *Millimeter Wave Properties of the Atmosphere: Laboratory Studies and Propagation Modeling*, Nat. Telecom. and Inform. Admin., NTIA Report 87-24, Boulder, Colorado, 1987.

[9] H. J. Liebe, "MPM—An Atmospheric Millimeter Wave Propagation Model," *Int. J. Infrared Millimeter Waves*, vol. 10, pp. 631–650, 1989.

[10] D. C. Hogg, F. O. Guiraud, J. B. Snider, M. T. Decker, and E. R. Westwater, "A Steerable Dual Channel Microwave Radiometer for Measurement of Water Vapor and Liquid in the Troposphere," *J. Appl. Meteorol.*, vol. 22, pp. 789–806, 1983.

[11] E. R. Westwater, J. B. Snider, and M. J. Falls, "Ground-Based Radiometric Observations of Atmospheric Emission and Attenuation at 20.6, 31.65, and 90.0 GHz: A Comparison of Measurements and Theory," *IEEE Trans. Antennas Propag.*, vol. AP-38, pp. 1569-1580, 1990.

[12] S. J. Keihm, "Atmospheric Absorption from 20–32 GHz: Radiometric Constraints on the Vapor and Oxygen Components," *Proc. Specialist Meeting on Microwave Radiometry and Remote Sensing Applications*, pp. 211–218, Boulder, Colorado, 1992.

[13] C. E. Kuehn, G. Elgered, J. M. Johansson, T. A. Clark, and B. O. Ronnang, "A Microwave Radiometer Comparison and Its Implication for the Accuracy of Wet Delays," in *Space Geodesy and Geodynamics*, edited by D. E. Smith, K. Kadinski-Cade, and T. L. Fischetti, AGU Monograph, 1993.

[14] Y. Han, J. B. Snider, E. R. Westwater, S. H. Melfi, and R. A. Ferrare, "Observations of Water Vapor by Ground-Based Microwave Radiometers and Raman Lidar," *J. Geophys. Res.*, vol. 99, pp. 18,695–18,702, 1994.

[15] W. E. Hoehne, *Precision of National Weather Service Upper Air Measurements*, NOAA Technical Memorandum NWS T&ED-16, 1980.

[16] B. E. Schwartz and C. A. Doswell III, "North American Rawinsonde Observations: Problems, Concerns, and a Call to Action," *Bull. Am. Meteor. Soc.*, vol. 72, pp. 1885–1896, 1991.

[17] W. P. Elliot and D. J. Gaffen, "On the Utility of Radiosonde Humidity Archives for Climate Studies," *Bull. Am. Meteor. Soc.*, vol. 72, pp. 1507–1520, 1991.

[18] J. C. Liljegren and B. M. Lesht, "Measurements of Integrated Water Vapor and Cloud Liquid Water from Microwave Radiometers at the DOE ARM Cloud and Radiation Testbed in the U.S. Southern Great Plains," *Proceedings of IGARSS'96*, Lincoln, Nebraska, pp. 1675–1677, 1996.

[19] R. J. Hill, "Water Vapor-Absorption Line Shape Comparison Using the 22 GHz Line: The Van Vleck–Weisskopf Shape Affirmed," *Radio Sci.*, vol. 21, pp. 447–451, 1986.

[20] S. L. Cruz-Pol, C. S. Ruf, and S. J. Keihm, "Improved 20- to 32-GHz Atmospheric Absorption Model," *Radio Sci.*, vol. 33, no. 5, pp. 1319–1333, 1998.

[21] Y. E. Bar-Sever, P. M. Kroger, and J. A. Borjesson, "Estimating Horizontal Gradients of Tropospheric Path Delay with a Single GPS Receiver," *J. Geophys. Res.*, vol. 103, pp. 5019–5035, 1998.

[22] J. Saastamoinnen, "Atmospheric Correction for the Troposphere and Stratosphere in Radio Ranging of Satellites," in *The Use of Artificial Satellites for Geodesy*, Geophysics Monograph, Series 15, American Geophysics Union, pp. 247–251, 1972.

[23] J. M. Duan, M. Bevis, P. Fang, Y. Bock, S. Chiswell, S. Businger, C. Rocken, F. Solheim, T. Van Hove, R. Ware, S. McClusky, T. Herring, and R. King, "GPS Meteorology: Direct Estimation of the Absolute Value of Precipitable Water," *J. App. Meteor.*, vol. 35, no. 6, pp. 830–838, 1996.

[24] T. R. Emardson, G. Elgered, and J. M. Johansson, "Three Months Continuous Monitoring of the Atmospheric Water Vapor with a Network of Global Positioning Receivers," *J. Geophys. Res.*, vol. 103, D2, pp. 1807–1820, 1998.

[25] P. Tregoning, R. Boers, D. M. O'Brien, and M. Hendy, "Accuracy of Absolute Precipitable Water Estimates from GPS Observations," *J. Geophys. Res.*, vol. 103, pp. 28,701–28,710, 1998.

[26] A. E. Niell, "Global Mapping Functions for the Atmospheric Delay at Radio Wavelengths," *J. Geophys. Res.*, vol. 101, pp. 3227–3246, 1996.

[27] G. Boudouris, "On the Index of Refraction of Air, the Absorption and Dispersion of Centimeter Waves by Gasses," *J. Res. Natl. Bur. Stand.*, Section D, vol. 67, pp. 631–684, 1963.

[28] R. J. Hill, R. S. Lawrence, and J. T. Priestly, "Theoretical and Calculational Aspects of the Radio Refractive Index of Water Vapor," *Radio Sci.*, vol. 17, pp. 1251–1257, 1982.

[29] H. J. Liebe, P. W. Rosenkranz, and G. A. Hufford, "Atmospheric 60-GHz Oxygen Spectrum: New Laboratory Measurements and Line Parameters," *J. Quant. Spectrosc. Radiat. Transfer*, vol. 48, pp. 629–643, 1992.

[30] J. F. Zumberge, M. B. Heflin, D. C. Jefferson, M. M. Watkins, and F. H. Webb, "Precise Point Positioning for the Efficient and Robust Analysis of GPS Data from Large Networks," *J. Geophys. Res.*, vol. 102, no. B3, pp. 5005–5017, 1997.

[31] Y. Han and E. R. Westwater, "Analysis and Improvement of Tipping Calibration for Ground-Based Microwave Radiometers," *IEEE Trans. Geosci. Remote Sens.*, vol. 38, pp. 1260–1277, 2000.

[32] M. A. Janssen, "A New Instrument for the Determination of Radio Path Delay due to Atmospheric Water Vapor," *IEEE Trans. Geosci. Remote Sens.*, vol. GE-23, no. 4, pp. 485–490, 1985.

[33] G. M. Resch, M. C. Chavez, N. I. Yamane, K. M. Barbier, and R. C. Chandlee, *Water Vapor Radiometry Research and Development Phase Final Report*, JPL Publication 85-14, Jet Propulsion Laboratory, Pasadena, California, April, 1985.

[34] J. Liljegren, "Two-Channel Microwave Radiometer for Observations of Total Column Precipitable Water Vapor and Cloud Liquid Water Path," paper presented at the Fifth Symposium on Global Change Studies, American Meteorological Society, Nashville, Tennessee, January 23–28, 1994.

Appendix

18 to 32 Gigahertz Water Vapor Absorption Model Parameterization

The formulation presented below represents an abbreviated version of the Liebe87 [8] vapor-absorption model with the addition of variable parameters for scaling the 22.2 GHz line strength and width and the empirical continuum contribution. The model validity is restricted to the 18 to 32 GHz spectral range.

Let

$T =$ temperature, K

$P =$ total pressure, mb

$\rho_v =$ vapor density, g/m^3

$\nu =$ frequency, GHz

$T_N = 300/T =$ normalized temperature

$P_v = \rho_v/(0.7223 \times T_N) =$ vapor pressure, mb

$P_d = P - P_v =$ dry pressure, mb

Then, the vapor absorption coefficient in nepers/km $= \alpha(\nu, T, P, \rho_v) = \alpha_R + \alpha_C =$ the sum of the resonance and continuum terms, where

$$\alpha_R = 0.0419 \times \nu^2 \times f_L \times f_W$$

$$\alpha_C = 0.0419 \times \nu^2 \times f_C$$

with

$$f_L = 0.0109 \times C_L \times P_v \times T_N^{3.5} \times \exp[2.143 \times (1 - T_N)]$$

$$f_W = \frac{W}{\nu_0} \times \left\{ \frac{1}{(\nu_0 - \nu)^2 + W^2} + \frac{1}{(\nu_0 + \nu)^2 + W^2} \right\}$$

$$f_C = 0.1 \times C_C \times P_v \times T_N^{2.5} \times \left([1.13 \times 10^{-7}] \times P_d \times T_N^{0.5} + [3.57 \times 10^{-6}] \times P_v \times T_N^8 \right)$$

and

$$W = \text{line width} = 0.002784 \times C_W \times \left(P_d \times T_N^{0.6} + 4.8 \times P_v \times T_N^{1.1} \right)$$

$$\nu_0 = \text{resonance frequency} = 22.235$$

The scale parameters C_L, C_W, and C_C can be adjusted to modify the line strength, line width, and continuum component, respectively. Values of $C_L = 1.0$, $C_W = 1.0$, and $C_C = 1.2$ produce a vapor absorption model that agrees with the Liebe87 model to within 0.5 percent over the 18 to 32 GHz spectral range.